

Stability of ZnSe-Passivated Laser Facets Cleaved in Air and in Ultra-High Vacuum

Jos E. Boschker¹, Uwe Spengler, Peter Ressel¹, Martin Schmidbauer², Anna Mogilatenko, and Andrea Knigge¹

Abstract—Catastrophic optical mirror damage (COMD) is one of the main failure mechanisms limiting the reliability of GaAs based laser diodes. Here, we compare the facet stability of ZnSe-passivated ridge-waveguide lasers (RWLs) that are cleaved in air and subsequently cleaned using atomic hydrogen with RWLs that are cleaved in ultra-high vacuum. RWLs cleaved in ultra-high vacuum show a superior performance and reach power densities up to 58 MW/cm² under extended continuous wave operation at 1064 nm. This is attributed to the reduction of defects at the interface between ZnSe and the cleaved facet as evidenced by transmission electron microscopy and X-ray diffraction.

Index Terms—Diode lasers, reliability, semiconductor lasers, quantum well lasers.

I. INTRODUCTION

GaAs based edge emitting semiconductor laser diodes are among the most efficient light sources currently available, resulting in the widespread adoption of laser bars for laser pumping and material processing. Moreover, the unrivaled efficiency of GaAs based edge emitting semiconductor lasers is also highly beneficial for future LiDAR applications [1]. Therefore, great efforts have been made during the last years to improve the maximum power output and efficiency of semiconducting lasers, resulting in a power of more than 1 kW from single 1 cm wide laser bars operating in the spectral range from 780–970 nm [2]. Emerging applications exploiting quantum phenomena, such as space-born Bose-Einstein condensation [3], require miniaturized high brightness light sources and therefore rely on GaAs based wavelength stabilized ridge-waveguide lasers (RWLs). Common to all these applications is the need for a high reliability at increasingly higher output powers.

Beside gradual degradation of the output power during operation, catastrophic optical damage (COD) can destroy a diode laser and therefore limits the reliability. One of the main COD

mechanisms of semiconductor lasers at these high-power levels is catastrophic optical mirror damage (COMD). During the last decades numerous solutions to improve laser facet stability have been developed. These include, but are not limited to, the E2 passivation process [4], quantum well intermixing [5], vacuum cleaving with ZnSe-passivation [6] or atomic hydrogen cleaning with epitaxial ZnSe-passivation [7]. Using the last method, it is possible to obtain lifetimes in excess of 20.000 hours for 980 nm RWLs operating at 1 W and in excess of 4000 hours operating at 2 W, i.e., close to the thermal rollover limit (trl). These output powers correspond to peak power densities at the facet in the range of 20 MW/cm² and 40 MW/cm², respectively. Even though such results are excellent, it is desirable to further improve the facet stability. One possible factor that could influence the facet stability of the ZnSe-passivation process is the incomplete removal of oxide from the (Al,Ga)As waveguides and cladding layers. Unfortunately, AlO_x cannot be removed completely from the facet using atomic hydrogen cleaning. Alternatively, sputter cleaning can be used to remove the AlO_x from the facets. However, that introduces defects in the laser facet. A laser facet completely free from oxide and other defects can only be obtained using cleaving in ultra-high vacuum (UHV) with subsequent epitaxial growth of ZnSe. In this paper we describe our investigations of the stability of laser facets cleaved in UHV and subsequently passivated by ZnSe. We compare these results with lasers cleaved in air, cleaned using atomic hydrogen and passivated by ZnSe.

Unfortunately, it is not possible to test the limits of the hydrogen cleaning passivation method or a possible improvement by using UHV-cleaving using 980 nm RWLs. This is due to the fact that the optical output power of our 980 nm RWLs is limited to 2 W due to thermal rollover and operating times in excess of 4000 hours can already be achieved at this output power using air-cleaving in combination with hydrogen cleaning followed by ZnSe passivation. It is thus not possible to increase the output power and longer lifetime measurements are also unpracticable. In order to overcome this limitation, we used RWLs that are more susceptible to COMD. We found that 1064 nm RWLs with double [8] and triple [9] quantum wells fail earlier during lifetime tests due to COMD and therefore used 980 nm and 1064 nm RWLs in this comparative study. Initial results of this study were presented at the ISLC [10]. Here, we provide additional structural as well as optoelectronic characterization of the two passivation techniques.

Manuscript received February 8, 2022; revised May 2, 2022; accepted May 18, 2022. Date of publication May 23, 2022; date of current version June 3, 2022. This work was supported by ERDF under Project 1.8/15. (Corresponding author: Jos E. Boschker.)

Jos E. Boschker, Uwe Spengler, Peter Ressel, Anna Mogilatenko, and Andrea Knigge are with the Ferdinand-Braun-Institut gGmbH Leibniz-Institut fuer Hoechstfrequenztechnik, 12489 Berlin, Germany (e-mail: jos.boschker@fbh-berlin.de; uwe.spengler@fbh-berlin.de; peter.ressel@fbh-berlin.de; anna.mogilatenko@fbh-berlin.de; andrea.knigge@fbh-berlin.de).

Martin Schmidbauer is with the Leibniz-Institut für Kristallzüchtung, 12489 Berlin, Germany (e-mail: martin.schmidbauer@ikz-berlin.de).

Digital Object Identifier 10.1109/JPHOT.2022.3176675

II. EXPERIMENTAL DETAILS

All ridge-waveguide lasers used in this work have a length of 3.9 mm and a width of 5 μm . The 980 nm and 1064 nm RWLs with a double quantum well are based on a 4.8 μm -wide asymmetric large optical cavity design (ASLOC) [8], whereas the 1064 nm RWLs with a triple quantum well are based on a 3.6 μm -wide symmetric super large optical cavity (SLOC) [9]. The SLOC structure has an approximately three times higher confinement factor compared to the ASLOC structure. Two types of approaches are used for passivating the laser facets. For the first approach the lasers are cleaved in air, stacked and loaded in an UHV MBE system (Veeco Gen 20A) where the oxide is removed from the facets using atomic hydrogen. The air exposure time was kept below 3 hours. After this cleaning an epitaxial ZnSe layer is grown on the facet using a temperature setpoint of 225 $^{\circ}\text{C}$ in order to passivate it [7]. For the second approach the laser bars are cleaved in an ultra-high vacuum MBE system (SVTA) and an epitaxial ZnSe layer is grown on the facets using a temperature setpoint of 250 $^{\circ}\text{C}$. In the remainder of this letter these two methods will be referred to as hydrogen cleaning and UHV cleaving, respectively. After the passivation optical coatings are deposited on the facets in order to set the reflectivities at 1.5% and 96% for the front and backside facet, respectively. Al_2O_3 was used for the low reflective front facet, whereas $\text{TiO}_2/\text{Al}_2\text{O}_3$ and $\text{Ta}_2\text{O}_5/\text{SiO}_2$ pairs were used for the high reflective backside facet.

The processed laser bars are separated into chips containing a single RWL. These chips are soldered p-side down on top of CuW heat spreaders and C-mounts that are used for the optical characterization and lifetimes measurements. The measurements are performed in continuous wave (CW) operation at 25 $^{\circ}\text{C}$.

Structural investigations of the laser diodes were carried out using scanning transmission electron microscopy (STEM, JEOL-2200FS) and high-resolution X-ray diffraction analysis (HR-XRD). Focused ion beam (FIB) technique was used to prepare thin cross-sectional lamellas containing the passivated laser facets. High angle annular dark-field (HAADF) STEM imaging, also known as Z-contrast imaging, was used to visualize structure of the layers and compositional homogeneity of the interfaces between the ZnSe passivation and the cleaved laser facets, whereas energy dispersive X-ray (EDX) spectroscopy was applied to reveal chemical elements constituting these interfaces. Additionally, selected area electron diffraction (SAED) patterns were acquired using parallel electron beam at different positions of ZnSe layers grown epitaxially on the laser facet.

High-resolution X-ray diffraction was performed using a commercial Rigaku SmartLab system operating at 9 kW. Behind a parabolic Göbel mirror, a 2 x Ge(220) channel-cut crystal is used to select the $\text{Cu-K}\alpha_1$ line ($\lambda = 1.5406 \text{ \AA}$) and collimate the useful beam to less than 0.008 $^{\circ}$. A two-dimensional area detector (HyPix 3000) was used to acquire 2θ - ω scans and two-dimensional reciprocal space maps.

III. RESULTS AND DISCUSSION

RWLs passivated using both methods were investigated using cross-sectional STEM. Fig. 1(a) shows a HAADF STEM image

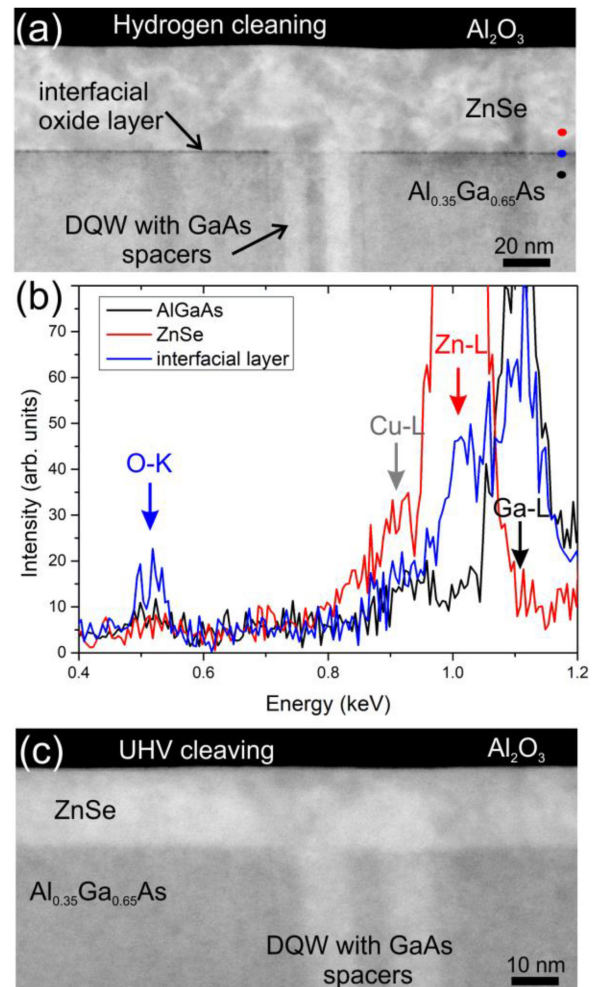


Fig. 1. HAADF STEM images of passivated facets in the quantum well region fabricated by hydrogen cleaning (a) and by cleaving in vacuum (c). EDX spectra of the points marked in (a) are shown in (b), demonstrating the presence of oxygen at the interface. The Cu-signal is due to the use of a copper ring for STEM investigations.

of a laser facet above the QW region for the sample cleaved in air and cleaned with atomic hydrogen. This image exhibits atomic number contrast (Z-contrast). There is a thin dark layer visible at the interface between the ZnSe layer and (Al,Ga)As. Such a layer can be attributed to a thin oxide layer. EDX measurements at different positions marked with the three dots in Fig. 1(a) were performed in order to verify this assumption, Fig 1(b). Oxygen enrichment was indeed found at the interface, demonstrating that the dark layer is caused by an oxide at the interface. The oxide is absent between the InGaAs quantum wells and ZnSe and between the GaAs spacers and ZnSe, but appears clearly visible between ZnSe and the (Al,Ga)As waveguide layers. This shows that the InGaAs and GaAs surface can be successfully cleaned from the native oxide. The presence of an oxide on top of (Al,Ga)As is caused by the formation of aluminum oxide on (Al,Ga)As, which is not removable using atomic hydrogen cleaning. In contrast, the passivated facet cleaved in UHV and the corresponding ZnSe layer on top of $\text{Al}_{0.35}\text{Ga}_{0.65}\text{As}$ show a different structure, Fig. 1(c). The oxide layer between (Al,Ga)As and ZnSe is not present.

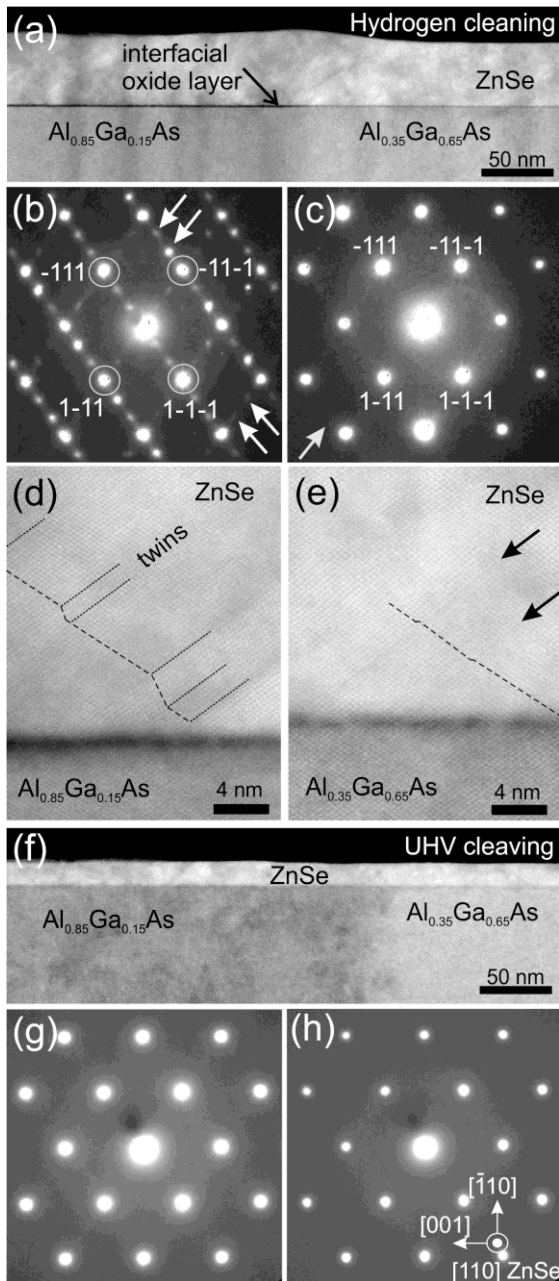


Fig. 2. STEM images and SAED-patterns of the ZnSe layer on the cladding and waveguide layers fabricated by hydrogen cleaning (a)–(e) and by cleaving in vacuum (f)–(h). SAED-patterns of ZnSe on $\text{Al}_{0.85}\text{Ga}_{0.15}\text{As}$ are shown in (b) & (g), whereas the SAED-patterns of ZnSe on $\text{Al}_{0.35}\text{Ga}_{0.65}\text{As}$ are shown in (c) & (h). The arrows in (b) point toward the additional diffraction spots caused by crystal twinning in the ZnSe layer, which is visible in (d). The arrow in (c) points toward the faint streaks indicative of such crystalline defects as stacking faults, shown in (e).

Since the oxide layer is formed during exposure of (Al,Ga)As facet to the air it is of interest to know the influence of the aluminum content on the oxide layer thickness and the structural quality of the ZnSe layer grown on top. Therefore, STEM images and SAED patterns were acquired in the facet region covering both the p-side cladding ($\text{Al}_{0.85}\text{Ga}_{0.15}\text{As}$) and waveguide ($\text{Al}_{0.35}\text{Ga}_{0.65}\text{As}$) layers. Fig. 2(a) shows a HAADF-STEM image of the ZnSe layer of a hydrogen cleaned facet in this region.

It can be seen that the remaining oxide thickness is larger on $\text{Al}_{0.85}\text{Ga}_{0.15}\text{As}$ compared to $\text{Al}_{0.35}\text{Ga}_{0.65}\text{As}$. This is consistent with the larger Al content of the cladding layer and hence stronger oxidation. Moreover, the ZnSe surface is found to be rougher on $\text{Al}_{0.85}\text{Ga}_{0.15}\text{As}$ compared to the ZnSe surface on $\text{Al}_{0.35}\text{Ga}_{0.65}\text{As}$.

Selective area electron diffraction (SAED) patterns were acquired for the ZnSe layers grown on $\text{Al}_{0.85}\text{Ga}_{0.15}\text{As}$ and $\text{Al}_{0.35}\text{Ga}_{0.65}\text{As}$ in order to investigate structural differences between ZnSe on the (Al,Ga)As layers with the different Al content. These are shown in Fig. 2(b) and (c), respectively. Bright diffraction spots corresponding to the zinc-blende structure of ZnSe viewed along the [110] zone axis are clearly visible and labelled accordingly. Between these bright diffraction spots there are strictly arranged spots with a lower intensity, as indicated by the white arrows. The appearance and arrangement of these additional diffraction spots is typical for crystal regions mirrored on the {111}-planes of the zinc-blende structure, indicating that the ZnSe layer on top of $\text{Al}_{0.85}\text{Ga}_{0.15}\text{As}$ contains a number of twins. Such microtwins together with stacking faults have been typically observed in ZnSe layers grown on GaAs substrates before [11]. The SAED-pattern for the ZnSe on $\text{Al}_{0.35}\text{Ga}_{0.65}\text{As}$ doesn't show any indication of twins. This shows that the density of twins is reduced on (Al,Ga)As layers with a reduced aluminum content and a smaller amount of AlO_x at the ZnSe/(Al,Ga)As interface. Nevertheless, faint stripes can be seen in the SAED on $\text{Al}_{0.35}\text{Ga}_{0.65}\text{As}$, indicated by the arrow in Fig. 2(c), indicative of crystalline defects, such as stacking faults. Indeed, HAADF STEM imaging at higher magnifications (Fig. 2(d) and (e)) revealed both types of the defects suggested from the SAED analysis: twins in ZnSe grown on strongly oxidized $\text{Al}_{0.85}\text{Ga}_{0.15}\text{As}$ and stacking faults on {111}-ZnSe planes in ZnSe grown on less oxidized $\text{Al}_{0.35}\text{Ga}_{0.65}\text{As}$ surface. These observations indicate that the crystal quality of the ZnSe layers strongly depends on the chemical composition and the crystalline quality of the (Al,Ga)As surface.

Looking at the STEM image and the corresponding SAED-patterns for the passivation obtained after UHV cleaving clear differences can be observed, Fig. 2(f)–(h). First of all, no oxide is observed between (Al,Ga)As and ZnSe, even for the cladding layer with an aluminium content of 85%. Secondly the additional diffraction peaks, corresponding to the twinning, were not observed in any of the SAED patterns, demonstrating that the UHV cleaved facet results in ZnSe passivation layers free from twins. The STEM investigations thus confirm that cleaving in UHV results in improved quality of the ZnSe layers on (Al,Ga)As as well as a reduction of the interfacial defects compared to cleaving in air and subsequent atomic hydrogen cleaning.

Additional information about the structural properties of the ZnSe layers was obtained by high resolution X-ray diffraction. Note that these measurements probe the properties of ZnSe on the facet of the GaAs substrate and not on the (Al,Ga)As layers of the laser diode. This is due to the spot size of the HR-XRD setup that is larger than the substrate thickness and thus cannot probe the laser diode itself. Even though it is not a direct probe of the ZnSe crystal structure on the laser diode, it can still provide a good indication of the quality of the ZnSe passivation, especially

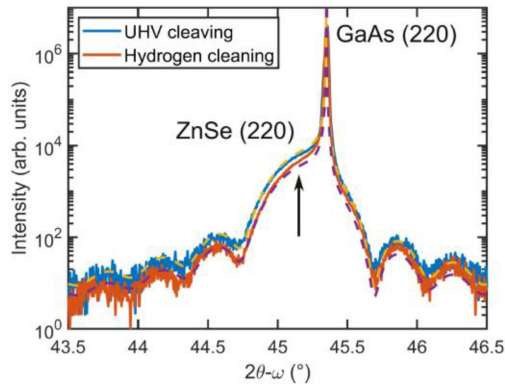


Fig. 3. HR-XRD 2θ - ω scans of ZnSe layers fabricated by hydrogen cleaning and by cleaving in vacuum. The dashed lines represent the simulations of the two data sets. The arrow points to difference between data and simulation, as explained in the text.

above the quantum well regions that are generally free from Al. Fig. 3 compares the HR-XRD 2θ - ω scans around the GaAs (220) reflection for ZnSe layers grown with both passivation techniques. Both measurements show clear substrate and film peaks as well as thickness fringes due to the finite thickness of the ZnSe layer. From simulations using dynamical X-ray diffraction theory that are fitted to the experimental data we determine the thickness of the ZnSe layer to be 24.5 nm and the ZnSe (110) lattice parameter to be 4.016 Å. This lattice parameter is 0.2% larger than the bulk value of ZnSe, consistent with 0.26% compressive lattice mismatch to GaAs and in good agreement with Ref. [12]. This shows that both methods result in ZnSe layers with a high structural quality. Nevertheless, two differences are observed. First of all, the intensity of the ZnSe diffraction peak is higher for the sample fabricated by UHV cleaving. Secondly, the fit to the data is nearly perfect for the sample fabricated by UHV cleaving. This indicates that the data can be well described by a homogeneous ZnSe layer on GaAs. For the sample produced by hydrogen cleaning, the fit to the data is not of the same quality and the measured and simulated curves don't overlap everywhere, as indicated by the arrow. This indicates that the ZnSe has a reduced quality and suggests that the ZnSe layer contains some defects. More detailed X-ray reciprocal space maps (not shown here) are indeed consistent with the presence of a small number of structural defects in this ZnSe layer. The presence of stacking faults and microtwins proven by SAED analysis on processed laser structures may be possible cause for these defects [13]. Possible origins for the defects in the ZnSe grown after hydrogen cleaning are the incomplete cleaning of the surface, an off-stoichiometric GaAs surface after cleaning, the presence of contaminations such as Si on the surface [14] or growth method related. Further investigations are needed in order to pinpoint the exact origin. The HR-XRD thus indicates that the ZnSe grown on GaAs after UHV cleaving have a higher structural quality than the ZnSe layers grown on GaAs after atomic hydrogen cleaning. For ZnSe grown on AlGaAs layers the difference in structural quality between the two methods is increased due to the stronger oxidation of the AlGaAs surface compared to that of GaAs and the presence of AlO_x at the

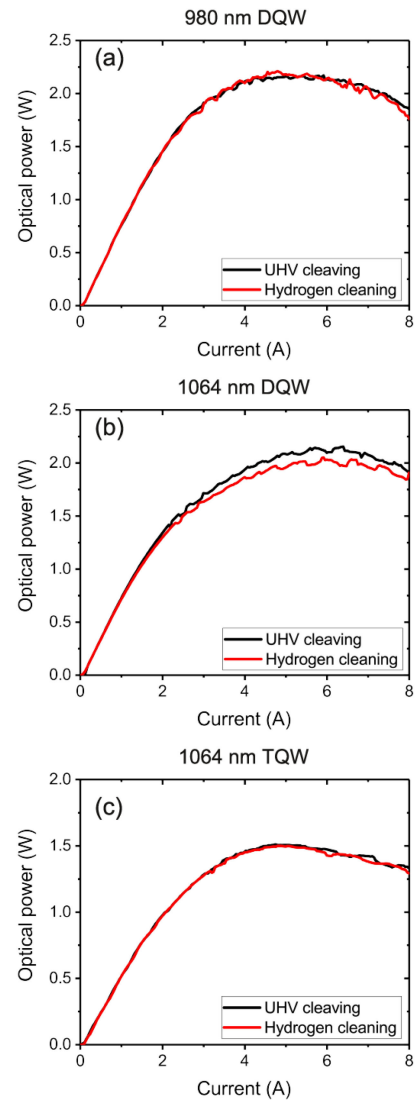


Fig. 4. Optical power as a function of current for the three types of RWLs investigated in this work: (a) 980 nm RWLs with a DQW, (b) 1064 nm RWLs with a DQW and (c) 1064 nm RWLs with a TQW. The maximum power of all RWLs is limited by thermal roll-over, regardless of passivation method.

AlGaAs/ZnSe interface after hydrogen cleaning. We expect that the presence of AlO_x is the defect that dominates the device lifetime.

Now we turn to the electro-optical characterization of the RWLs. Fig. 4 shows typical power-current-curves of the RWLs used in this study. We don't observe any COMD up to currents of 8A for all RWLs, regardless of the passivation technique. This value corresponds to a maximum current density of 4.1 kA/cm^2 and drives the RWLs well above the thermal rollover limit. It is observed that RWLs with the double quantum well emitting at 980 nm and 1064 nm have a maximum output power slightly above 2 W, whereas the maximum output power for the TQW RWLs is limited to approximately 1.5 W, indicating a reduced efficiency for these RWLs. In all cases the maximum power facet density exceeds 40 MW/cm^2 , as will be discussed in more detail later. The reduced efficiency of the TQW RWLs is caused by the larger internal absorption in the SLOC structure compared

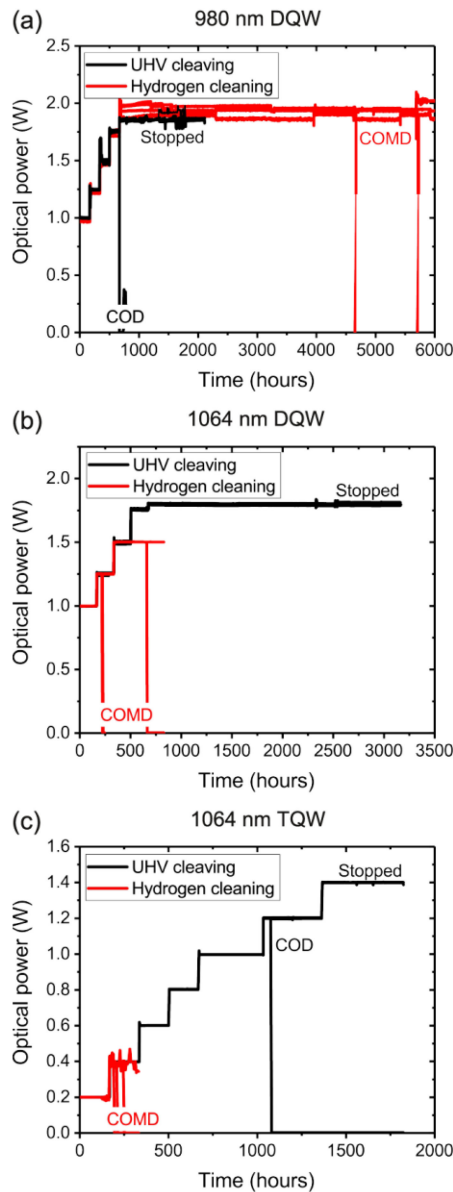


Fig. 5. Lifetime tests for the three types of RWLs investigated in this work: (a) 980 nm RWLs with a DQW, (b) 1064 nm RWLs with a DQW and (c) 1064 nm RWLs with a TQW. Improved lifetimes are observed for the RWLs cleaved in UHV.

to the ASLOC structure due to the thicker p-side (Al,Ga)As layers in the SLOC structure and by the larger current spreading for the SLOC RWLs compared to the ASLOC RWLs due to a larger residual layer thickness in the etched trenches defining the ridge.

After the initial characterization, lifetime measurements were performed on all types of RWLs in order to investigate the facet stability during continuous wave laser operation. For the lifetime test the output power was step-wise increased up to output powers close to the thermal rollover limit. The measurements for both types of passivation methods are compared in Fig. 5. Starting with the 980 nm RWLs we see that RWLs produced with both passivation methods can be operated with output powers above 1.75 W for more than 2000 hours, Fig. 5(a). For the RWLs

passivated by UHV cleaving a single failure is observed when the power is increased above 1.75 W. Since the facet of this RWL is free from any damage after this failure a COMD is excluded as a cause of the failure and the failure is marked as a COD event. Having reached the 2000 hours milestone without mirror damage, the lifetime test for the RWLs produced by UHV cleaving was stopped. For the 1064 nm RWLs, Fig. 5(b) and (c), we observe that the maximum output power of the RWLs passivated with the hydrogen cleaning process are decreased compared to the 980 nm RWLs. For the DQW it is around 1.5 W and for the TQW it is no more than 0.4 W. A possible origin of this reduction is the additional strain due to the increased Indium content in the 1064 nm QWs. This will result in an increased lattice relaxation of the QW at the facet and therefore more absorption, reducing the facet stability [15]. For the SLOC structure with TQW this effect is expected to be enhanced compared to a DQW, because of the extra QW and the higher confinement factor.

For the RWLs passivated by means of UHV cleaving no COMD is observed for output powers up to the thermal rollover limit. This demonstrates that the stability of facets passivated by UHV cleaving is enhanced with respect to hydrogen cleaning. More specifically, a more than three times higher facet stability is obtained for the 1064 nm RWLs with a TQW. Furthermore, it is observed that internal damage occurs at 1.2 W (COD) for this type of RWL, suggesting that bulk degradation becomes significant.

The lifetime tests thus demonstrate that RWLs with InGaAs quantum wells that were cleaved in UHV have an enhanced lifetime and can operate at higher output powers compared to RWLs cleaved in air and cleaned using atomic hydrogen. The fact that the initial power-current-curves are similar, indicates that the facet degradation of RWLs produced by UHV cleaving is reduced. We attribute this to the reduced interface defect density and the improved structural quality of the ZnSe obtained by UHV cleaving, as evidenced by the TEM and XRD investigations. The exact physical mechanism causing the degradation is however unclear. It is known that thermal stress can result in the exchange of Ga and Zn across the ZnSe/GaAs interface [16], [17]. Since Zn acts as an acceptor in InGaAs and (Al,Ga)As this would increase the optical absorption in the interface region and eventually contribute to lowering the COMD limit. The initial amount of Zn in the InGaAs/(Al,Ga)As layers would be similar for both types of passivation methods explaining the similar PI-curves.

Moreover, such a diffusion process could be enhanced by the presence of defects at the ZnSe/InGaAs (or (Al,Ga)As) interface [18], explaining the faster degradation of RWLs passivated using atomic hydrogen cleaning. Since the quantum well regions for both passivation methods are similar it is expected that the defects on (Al,Ga)As surface play an important role for the degradation of the RWLs. Having Zn as a possible contribution to the facet degradation in mind, it is important to note that Zn diffusion strongly depends on the number of Gallium interstitials. Excess gallium interstitials are typically formed during the growth of n-type III-V layers [19]. Optimizing the growth of the III-V diode structure with this in mind could improve the

facet stability even further. Alternatively, Zn(Se,S) mirror layers could be used, as they are shown to be more stable [17].

Based on lateral near field measurements and the calculated mode profile the power density at the facets was calculated. The maximum power densities of the 1064 nm RWLs are determined to be 58 and 42 MW/cm² for the DQW and TQW, respectively and 42 MW/cm² for the 980 nm RWLs. These power densities are well above peak power densities that can be reached with broad area emitters [20]. Given the lifetime improvements for RWLs using UHV cleaving, we expect that a similar improvement might be reached for broad area emitters. This is however subject of a future study.

V. CONCLUSION

The presented results demonstrate that the facet stability of ZnSe-passivated semiconductor lasers is improved by cleaving the lasers in UHV instead of cleaving in air with a subsequent atomic hydrogen cleaning. This suggests that interfacial defects put a limit on the facet stability of ZnSe passivated lasers. The demonstrated long lifetimes of 1064 nm RWLs are a key enabler for future space-born quantum technologies. Moreover, it is expected that this improvement can also occur for other laser types, such as broad area emitters, or lasers operating at other wavelengths and thus expands the possible applications of semiconducting lasers.

ACKNOWLEDGMENT

The authors would like to thank A. Maaßdorf for growing the epitaxial wafers, the process technology department for processing the wafers, C. Münnich, M. Engstermann, R. Selent and A. Abo Taqya for passivating and applying the optical coatings to the laser bars and our colleagues from the optoelectronics department for electrooptical characterization. Furthermore, the authors are grateful to the mounting and assembling department for mounting the RWLs and to J. Glaab and S. Ullrich for the lifetime measurements. Finally, the authors like to thank H. Wenzel for useful discussions.

REFERENCES

- [1] A. Knigge *et al.*, "Wavelength-stabilized high-pulse-power laser diodes for automotive LiDAR," *Phys. Status Solidi A*, vol. 215, no. 8, 2018, Art. no. 1700439, doi: [10.1002/pssa.201700439](https://doi.org/10.1002/pssa.201700439).
- [2] P. Crump and G. Tränkle, "A brief history of kilowatt-class diode-laser bars," *Novel-Plane Semicond. Lasers XIX*, vol. 11301, pp. 148–156, Apr. 2020, doi: [10.1117/12.2546010](https://doi.org/10.1117/12.2546010).
- [3] D. Becker *et al.*, "Space-borne Bose–Einstein condensation for precision interferometry," *Nature*, vol. 562, no. 7727, pp. 391–395, Oct. 2018, doi: [10.1038/s41586-018-0605-1](https://doi.org/10.1038/s41586-018-0605-1).
- [4] M. Gasser and E. E. Latta, "Method for mirror passivation of semiconductor laser diodes," U.S. Patent 5 144 634, Sep. 1, 1992.
- [5] B. S. Ooi *et al.*, "Selective quantum-well intermixing in GaAs-AlGaAs structures using impurity-free vacancy diffusion," *IEEE J. Quantum Electron.*, vol. 33, no. 10, pp. 1784–1793, Oct. 1997, doi: [10.1109/3.631284](https://doi.org/10.1109/3.631284).
- [6] N. Chand, W. S. Hobson, J. F. de Jong, P. Parayanthal, and U. K. Chakrabarti, "ZnSe for mirror passivation of high power GaAs based lasers," *Electron. Lett.*, vol. 32, no. 17, pp. 1595–1596, Aug. 1996, doi: [10.1049/el:19961062](https://doi.org/10.1049/el:19961062).
- [7] P. Ressel *et al.*, "Novel passivation process for the mirror facets of Al-free active-region high-power semiconductor diode lasers," *IEEE Photon. Technol. Lett.*, vol. 17, no. 5, pp. 962–964, May 2005, doi: [10.1109/LPT.2005.846750](https://doi.org/10.1109/LPT.2005.846750).
- [8] H. Wenzel *et al.*, "Fundamental-lateral mode stabilized high-power ridge-waveguide lasers with a low beam divergence," *IEEE Photon. Technol. Lett.*, vol. 20, no. 3, pp. 214–216, Feb. 2008, doi: [10.1109/LPT.2007.913328](https://doi.org/10.1109/LPT.2007.913328).
- [9] O. Brox *et al.*, "Integrated 1060nm MOPA pump source for high-power green light emitters in display technology," in *Proc. Novel In-Plane Semicond. Lasers VII*, Jan. 2008, pp. 346–353, doi: [10.1117/12.761210](https://doi.org/10.1117/12.761210).
- [10] J. E. Boschker, U. Spengler, P. Ressel, A. Mogilatenko, and A. Knigge, "Stability of ZnSe-passivated laser facets cleaved in air and in ultra-high vacuum," in *Proc. 27th Int. Semicond. Laser Conf.*, Oct. 2021, pp. 1–2, doi: [10.1109/ISLCS1662.2021.9615691](https://doi.org/10.1109/ISLCS1662.2021.9615691).
- [11] F. A. Ponce, W. Stutius, and J. G. Werthen, "Lattice structure at ZnSe-GaAs heterojunction interfaces prepared by organometallic chemical vapor deposition," *Thin Solid Films*, vol. 104, no. 1–2, pp. 133–143, Jun. 1983, doi: [10.1016/0040-6090\(83\)90554-0](https://doi.org/10.1016/0040-6090(83)90554-0).
- [12] H.-C. Ko, D.-C. Park, Y. Kawakami, S. Fujita, and S. Fujita, "Optimization of ZnSe growth on the cleavage-induced GaAs (1 1 0) surface by molecular-beam epitaxy," *J. Cryst. Growth*, vol. 178, no. 3, pp. 246–251, Jul. 1997, doi: [10.1016/S0022-0248\(96\)01126-8](https://doi.org/10.1016/S0022-0248(96)01126-8).
- [13] S. R. Vangala, D. Brinegar, V. L. Tassev, and M. Snure, "Thick hydride vapor phase epitaxial growth of ZnSe on GaAs (1 0 0) vicinal and orientation patterned substrates," *J. Cryst. Growth*, vol. 522, pp. 230–234, Sep. 2019, doi: [10.1016/j.jcrysgro.2019.06.032](https://doi.org/10.1016/j.jcrysgro.2019.06.032).
- [14] K. D. Choquette *et al.*, "GaAs surface reconstruction obtained using a dry process," *J. Appl. Phys.*, vol. 73, no. 4, pp. 2035–2037, Feb. 1993, doi: [10.1063/1.353148](https://doi.org/10.1063/1.353148).
- [15] A. Valster *et al.*, "Strain-overcompensated GaInP-AlGaInP quantum-well laser structures for improved reliability at high-output powers," *IEEE J. Sel. Topics Quantum Electron.*, vol. 3, no. 2, pp. 180–187, Apr. 1997, doi: [10.1109/2944.605653](https://doi.org/10.1109/2944.605653).
- [16] D. H. Mosca *et al.*, "Chemical and structural aspects of annealed ZnSe/GaAs(001) heterostructures," *J. Appl. Phys.*, vol. 92, no. 7, pp. 3569–3572, Oct. 2002, doi: [10.1063/1.1504175](https://doi.org/10.1063/1.1504175).
- [17] K. Ohmi, I. Suemune, T. Kanda, Y. Kan, and M. Yamanishi, "Lattice-mismatch enhanced diffusion at a ZnSe/GaAs interface - Increase of thermal stability in a lattice-matching system," *Jpn. J. Appl. Phys.*, vol. 26, no. 12A, Dec. 1987, Art. no. L2072, doi: [10.1143/JJAP.26.L2072](https://doi.org/10.1143/JJAP.26.L2072).
- [18] T. Kanda, I. Suemune, K. Yamada, Y. Kan, and M. Yamanishi, "Thermal stability of nearly lattice-matched ZnSSe/GaAs interface grown by MOVPE," *J. Cryst. Growth*, vol. 93, no. 1–4, pp. 662–666, Jan. 1988, doi: [10.1016/0022-0248\(88\)90600-8](https://doi.org/10.1016/0022-0248(88)90600-8).
- [19] D. G. Deppe, "Thermodynamic explanation to the enhanced diffusion of base dopant in AlGaAs-GaAs npn bipolar transistors," *Appl. Phys. Lett.*, vol. 56, no. 4, pp. 370–372, Jan. 1990, doi: [10.1063/1.102788](https://doi.org/10.1063/1.102788).
- [20] P. Crump *et al.*, "20W continuous wave reliable operation of 980nm broad-area single emitter diode lasers with an aperture of 96um," in *Proc. High-Power Diode Laser Technol. Appl. VII*, Feb. 2009, pp. 315–323, doi: [10.1117/12.807263](https://doi.org/10.1117/12.807263).